Supporting information:

Anomalous Jahn-Teller behavior in manganese-based mixed-phosphate cathode for sodium ion batteries

Hyungsub Kim,[†ab] Gabin Yoon,[†ab] Inchul Park,[ab] Kyu-Young Park,[ab] Byungju Lee,[ab] Jongsoon Kim,[ac] Young-Uk Park,[a] Sung-Kyun Jung,[ab] Hee-Dae Lim,[a] Docheon Ahn,[d] Seongsu Lee [c] and Kisuk Kang [ab]*

[a] Department of Materials Science and Engineering, Research Institute of Advanced Materials, Seoul National University, 599 Gwanak-ro, Gwanak-gu, Seoul 151-742, Republic of Korea

[b] Center for Nanoparticle Research at Institute for Basic Science (IBS), Seoul National University, 599 Gwanak-ro, Gwanak-gu, Seoul 151-742, Republic of Korea

[c] Korea Atomic Energy Research Institute, P.O. Box 105, Daejeon 305-600, Republic of Korea

[d] Beamline Research Division, Pohang Accelerator Laboratory, Pohang 790-784, Republic of Korea

*Corresponding author: Kisuk Kang (matlgen1@snu.ac.kr)

[†]These authors contributed equally to this paper.

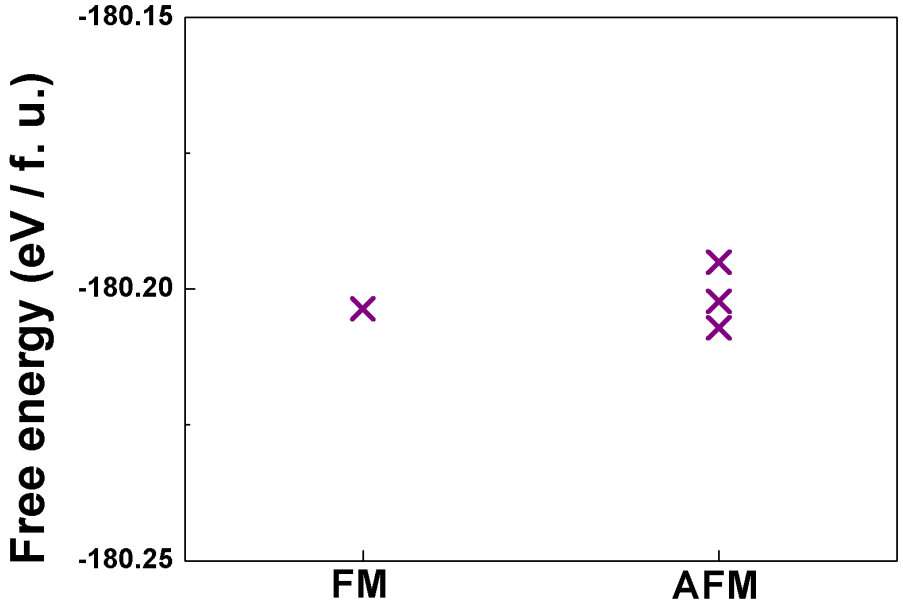

Figure S1. Free energies of $Na_4Mn_3(PO_4)_2P_2O_7$ with various magnetic configurations.

The electrochemical performances of $Na_4Mn_3(PO_4)_2(P_2O_7)$ in three types of electrolyte; 1M $NaBF_4$ in EC/PC (1:1 v/v), 1M $NaClO_4$ in EC/PC (1:1 v/v) and 1M $NaPF_6$ in EC/PC (1:1 v/v)

We compared three types of electrolyte, which are (i) 1M $NaBF_4$ in EC/PC (1:1 v/v), (ii) 1M $NaClO_4$ in EC/PC (1:1 v/v) and (iii) 1M $NaPF_6$ in EC/PC (1:1 v/v). The electrochemical profiles of $Na_4Mn_3(PO_4)_2(P_2O_7)$ electrode at the slow current rate of C/20 were very similar in three different electrolytes, as shown in Fig. S2a. Almost same capacity was delivered at the initial charge and subsequent cycles regardless of dissolved Na salts in electrolytes. The electrode operation in 1M $NaPF_6$ in EC/PC (1:1 v/v) electrolyte exhibits slightly better electrochemical performances at a low current rate of C/20 and room temperature (RT) than that in 1M $NaBF_4$ in EC/PC (1:1 v/v) electrolyte, while comparably poor electrochemical activity was confirmed in $NaClO_4$ electrolyte during discharge reaction. Fig. S2b illustrates the cycle retention of $Na_4Mn_3(PO_4)_2(P_2O_7)$ at C/20 and RT in three different types of electrolyte. The stable cycle performances with a retention of approximately 90 % was confirmed from both $NaBF_4$ and $NaPF_6$ electrolytes, while the electrode operation in $NaClO_4$ electrolyte shows comparably poor cycle retention after 10 cycles. We speculate that this cycle degradation is attributed to the residual water contents in $NaClO_4$ electrolyte. We carefully dried the Na salts of $NaPF_6$, $NaBF_4$ and $NaClO_4$ in 180ºC vacuum oven before dissolving in EC/PC solvents, however, the large amount of water contents were still detected from $NaClO_4$ (272 ppm) electrolyte by using Karl Fisher titration technique. On the other hand, the water contents in $NaPF_6$ and $NaBF_4$ electrolytes were determined to be 2.8 ppm and <1ppm, respectively. It is well known that dehydrating or drying $NaClO_4$ salt is challenging compared to other electrolyte salts [*J. Mater. Chem.* 2015, **3**, 22-42.], and for this reason, we believe that the dehydration of $NaClO_4$ salt was not sufficient enough to prevent side

reactions during electrochemical cycling in Na-ion cells.

The electrochemical properties of $Na_4Mn_3(PO_4)_2(P_2O_7)$ electrode at 1C and 60ºC shown in Fig. S2c also suggest that $NaPF_6$ and $NaBF_4$ electrolytes are suitable electrolytes for Na rechargeable batteries compared to $NaClO_4$ electrolyte. Almost same capacity was delivered at the initial charge in three electrolytes, and the highest discharge capacity was delivered from the cell using $NaPF_6$ as an electrolyte salt. However, the severe cycle degradation was found from both $NaClO_4$ and $NaPF_6$ electrolytes (See Fig. S2d). Only 5 % and 38 % of the initial capacity was retained after 20 cycles from the 60ºC cell using $NaClO_4$ and $NaPF_6$ electrolytes, respectively. We believe that the capacity degradation from these electrolytes may arise from the side reaction upon electrochemical cycling related to the water contents in the electrolytes. The poor cycle stability of the electrode in $NaClO_4$ electrolyte is attributed to the large amount water contents (272 ppm) in $NaClO_4$ electrolyte which may induces the side reaction during electrochemical cycling as previously mentioned. Although the water content in $NaPF_6$ electrolyte was 2.8 ppm, it may not be low enough to prevent side reactions during electrochemical cycling in high temperature Na-ion cells. Also, the possible impurities in $NaPF_6$ precursors such as Na_2PO_3F or NaF could be the reason of instability of the cell operation at 60ºC, while we used a $NaPF_6$ salt with the highest purity (99 %, Alfa Aesar) available. [*Phys. Chem. Chem. Phys.* 2014, **16**, 1987.]

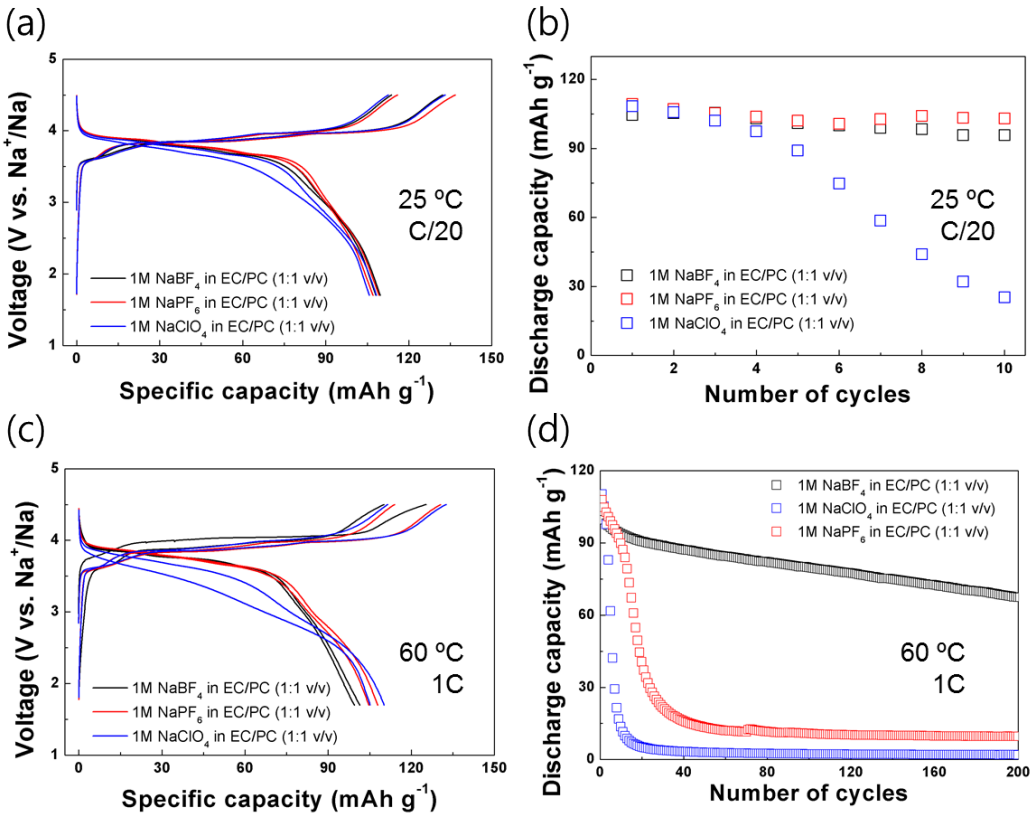

Figure S2. (a) Galvanostatic charge/discharge profiles and (b) cycle performances of $Na_4Mn_3(PO_4)_2(P_2O_7)$ electrode at a current rate of C/20 in three electrolytes using different Na salts; 1M $NaBF_4$ in EC/PC (1:1 v/v), 1M $NaClO_4$ in EC/PC (1:1 v/v) and 1M $NaPF_6$ in EC/PC (1:1 v/v). (c) Galvanostatic charge/discharge profiles and (b) cycle performances of $Na_4Mn_3(PO_4)_2(P_2O_7)$ electrode at a current rate of 1C in 60 ºC cells.

Table S1. The structural data on $Na_4Mn_3(PO_4)_2(P_2O_7)$ analyzed using Rietveld refinement of the X-ray diffraction (XRD) and neutron diffraction (ND) patterns. Details of the measurement conditions, lattice parameters, reliability factors, atomic positions and bond valence data are also listed.

Formula	$Na_4Mn_3(PO_4)_2(P_2O_7)$
Crystal system	Orthorhombic
Space group	$Pn2_1a$ (No. 33)
Lattice parameters	
a (Å)	18.02651 (7)
b (Å)	6.65673 (2)
c (Å)	10.76886 (4)
Unitcell volume (Å^3)	1290.07 (8)
Source	X-ray
Temperature (K)	300
Wave length (Å)	1.54950
2θ range (°)	10 – 100
Number of data points	12045
Number of reflections	1316
R_p (%)	6.84
R_{wp} (%)	9.82
R_I (%)	3.53
R_F (%)	2.14

Formula	$Na_4Mn_3(PO_4)_2(P_2O_7)$
Crystal system	Orthorhombic
Space group	$Pn2_1a$ (No. 33)
Lattice parameters	
a (Å)	18.0201 (7)
b (Å)	6.6508 (2)
c (Å)	10.7642 (4)
Unitcell volume (Å^3)	1290.07 (8)
Source	Neutron
Temperature (K)	300
Wave length (Å)	1.834333
2θ range (°)	10 – 100
Number of data points	0 – 180
Number of reflections	3200
R_p (%)	956
R_{wp} (%)	3.25
R_I (%)	4.22
R_F (%)	3.11

Atom	*x* (Å)	*y* (Å)	*z* (Å)	B_{iso}	Occupancy
Mn1	0.3435 (7)	0.060 (4)	0.5087 (17)	0.80 (17)	1.00
Mn2	0.1436 (7)	0.538 (4)	0.4837 (17)	0.80 (17)	1.00
Mn3	0.2443 (9)	0.272 (3)	0.741 (2)	0.80 (17)	1.00
P1	0.2991 (5)	0.547 (3)	0.5044 (13)	0.26 (9)	1.00
P2	0.1806 (5)	0.032 (3)	0.4770 (10)	0.26 (9)	1.00
P3	0.5603 (6)	0.422 (3)	0.7452 (12)	0.26 (9)	1.00
P4	0.4455 (5)	0.121 (3)	0.7265 (11)	0.26 (9)	1.00
Na1	0.5033 (12)	0.788 (4)	0.9823 (11)	0.34 (13)	1.00
Na2	0.2862 (7)	0.795 (3)	0.7513 (20)	0.34 (13)	1.00
Na3	0.3985 (8)	0.408 (3)	0.2602 (18)	0.34 (13)	1.00
Na4	0.4674 (10)	0.63488	0.5492 (14)	0.34 (13)	1.00
O1	0.2435 (6)	0.516 (3)	0.6134 (11)	1.19 (5)	1.00
O2	0.3507 (7)	0.375 (3)	0.4869 (11)	1.19 (5)	1.00
O3	0.3433 (6)	0.747 (3)	0.5330 (11)	1.19 (5)	1.00
O4	0.2528 (6)	0.564 (3)	0.3836 (10)	1.19 (5)	1.00
O5	0.2329 (6)	0.075 (3)	0.6006 (10)	1.19 (5)	1.00
O6	0.1279 (6)	-0.144 (3)	0.5032 (13)	1.19 (5)	1.00
O7	0.2357 (6)	0.011 (3)	0.3779 (12)	1.19 (5)	1.00
O8	0.1404 (7)	0.230 (3)	0.4496 (10)	1.19 (5)	1.00
O9	0.4784 (6)	0.336 (3)	0.7040 (9)	1.19 (5)	1.00
O10	0.5574 (6)	0.522 (3)	0.8691 (9)	1.19 (5)	1.00
O11	0.6201 (5)	0.242 (3)	0.7406 (12)	1.19 (5)	1.00
O12	0.5755 (5)	0.573 (3)	0.6450 (9)	1.19 (5)	1.00
O13	0.4670 (6)	0.048 (3)	0.8631 (11)	1.19 (5)	1.00
O14	0.3615 (5)	0.132 (3)	0.7116 (10)	1.19 (5)	1.00
O15	0.4792 (6)	-0.016 (3)	0.6360 (12)	1.19 (5)	1.00

Atom	Coordination number	Average Distance (Å)	Expected valence	Bond valence Summation
Mn1	6.00	2.22 (1)	2.00	1.95 (6)
Mn2	6.00	2.23 (1)	2.00	1.91 (6)
Mn3	6.00	2.16 (1)	2.00	2.28 (7)
P1	4.00	1.54 (1)	5.00	4.9 (1)
P2	4.00	1.55 (1)	5.00	4.9 (1)
P3	4.00	1.56 (1)	5.00	4.7 (1)
P4	4.00	1.54 (1)	5.00	5.0 (1)
Na1	6.00	2.40 (1)	1.00	1.26 (4)
Na2	7.00	2.53 (1)	1.00	1.03 (3)
Na3	5.00	2.47 (1)	1.00	0.78 (3)
Na4	6.00	2.492 (8)	1.00	1.04 (3)
O1	4.00	2.12 (1)	-2.00	-2.00 (6)
O2	4.00	2.25 (1)	-2.00	-2.0 (1)
O3	4.00	2.16 (1)	-2.00	-1.88 (9)
O4	4.00	2.06 (1)	-2.00	-2.17 (7)
O5	4.00	2.14 (1)	-2.00	-1.86 (6)
O6	3.00	1.99 (2)	-2.00	-1.90 (9)
O7	4.00	2.11 (1)	-2.00	-2.25 (7)
O8	4.00	2.20 (1)	-2.00	-2.0 (1)
O9	3.00	1.94 (1)	-2.00	-2.19 (9)
O10	4.00	2.14 (1)	-2.00	-2.10 (8)
O11	3.00	2.04 (1)	-2.00	-1.60 (7)
O12	4.00	2.11 (1)	-2.00	-2.16 (9)
O13	4.00	2.15 (1)	-2.00	-1.78 (6)
O14	4.00	2.19 (1)	-2.00	-1.90 (5)
O15	4.00	2.23 (1)	-2.00	-1.98 (9)

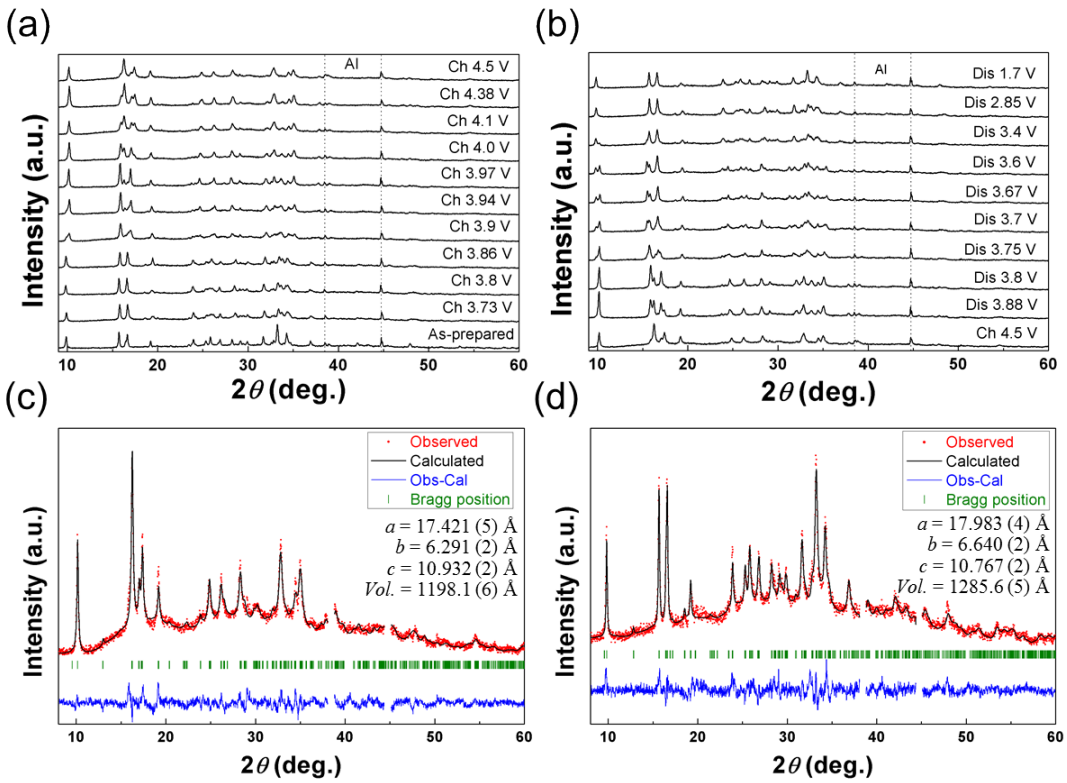

Figure S3. *Ex situ* XRD patterns of $Na_4Mn_3(PO_4)_2(P_2O_7)$ during (a) charge and (b) discharge. Rietveld refinement of the XRD patterns of (c) fully charged and (d) discharged electrodes. The R-factors of the fully charged electrodes were R_p = 4.91%, R_{wp} = 6.27%, R_I = 5.24% and R_F = 3.06%; those of the discharged electrode were R_p = 4.99%, R_{wp} = 6.33%, R_I = 8.37% and R_F = 4.81%.

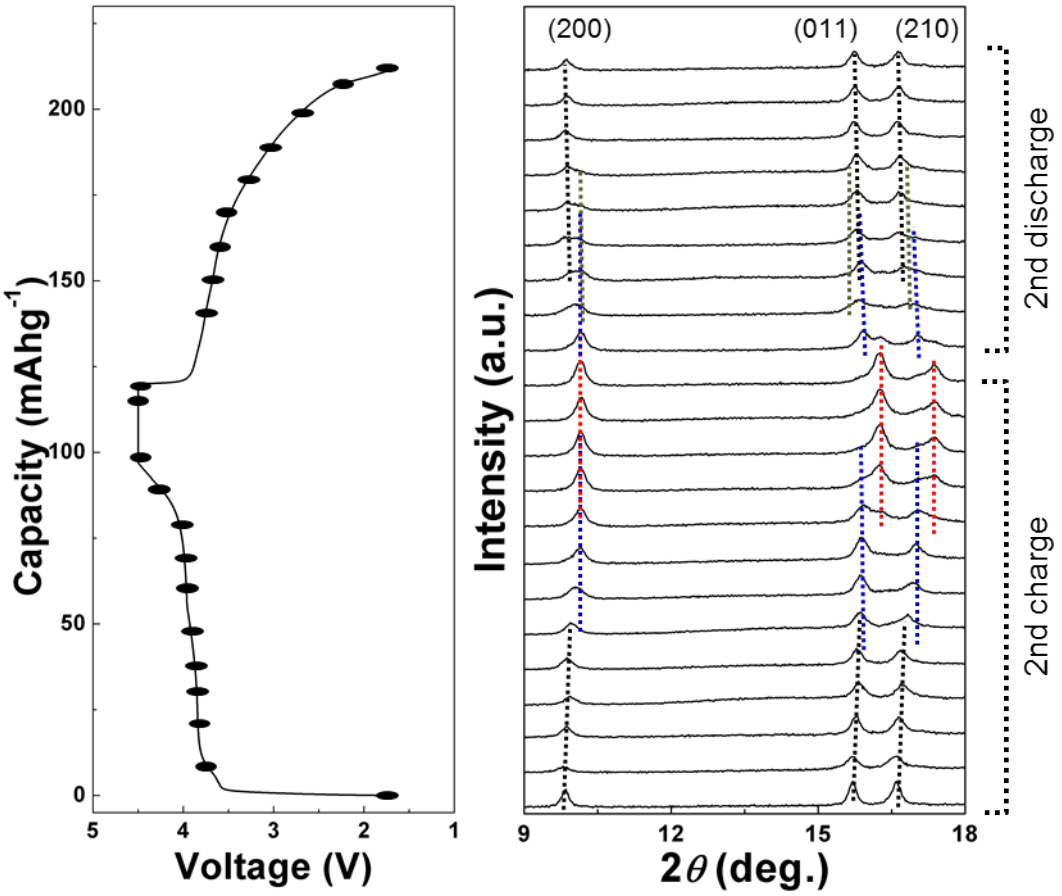

Figure S4. *Ex situ* XRD patterns of $Na_{4-x}Mn_3(PO_4)_2(P_2O_7)$ during the second charge/discharge cycle. The black, red, blue and green dotted curves corresponds to the α-, β-, γ- and δ-phases, respectively.

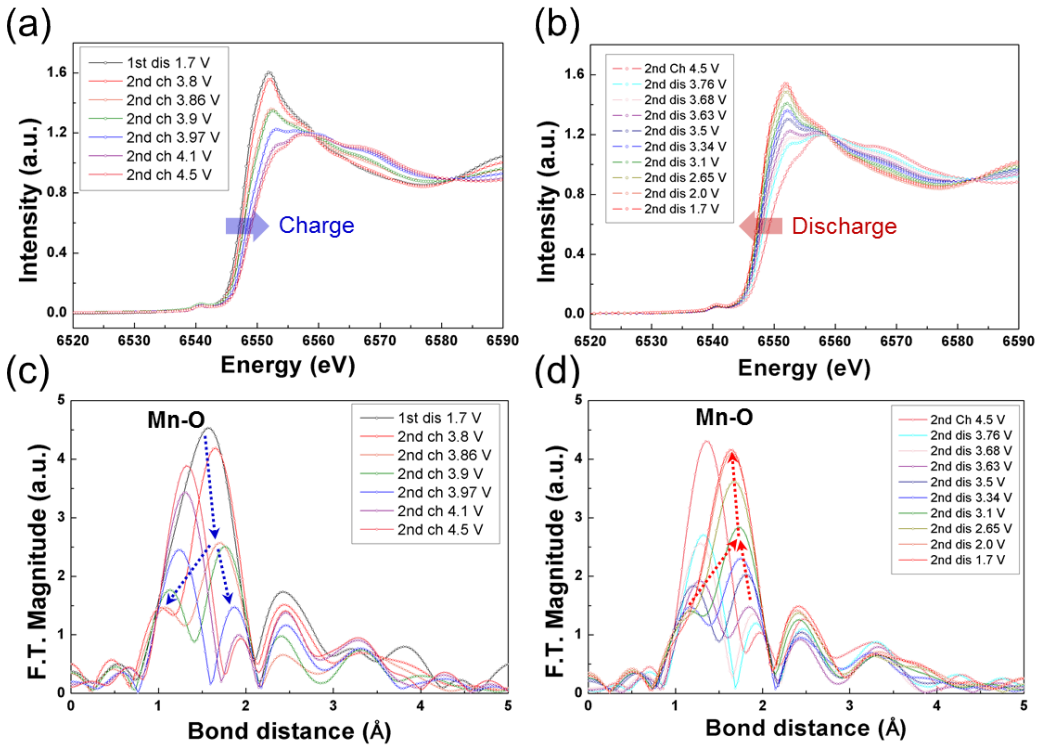

Figure S5. XANES spectra of the *ex situ* electrode samples of $Na_{4-x}Mn_3(PO_4)_2(P_2O_7)$ ($0 \leq x \leq 3$) during (a) the second charging and (b) discharging. *Ex situ* EXAFS spectra of $Na_{4-x}Mn_3(PO_4)_2(P_2O_7)$ ($0 \leq x \leq 3$) electrode samples (c) during the second charging and (d) discharging.

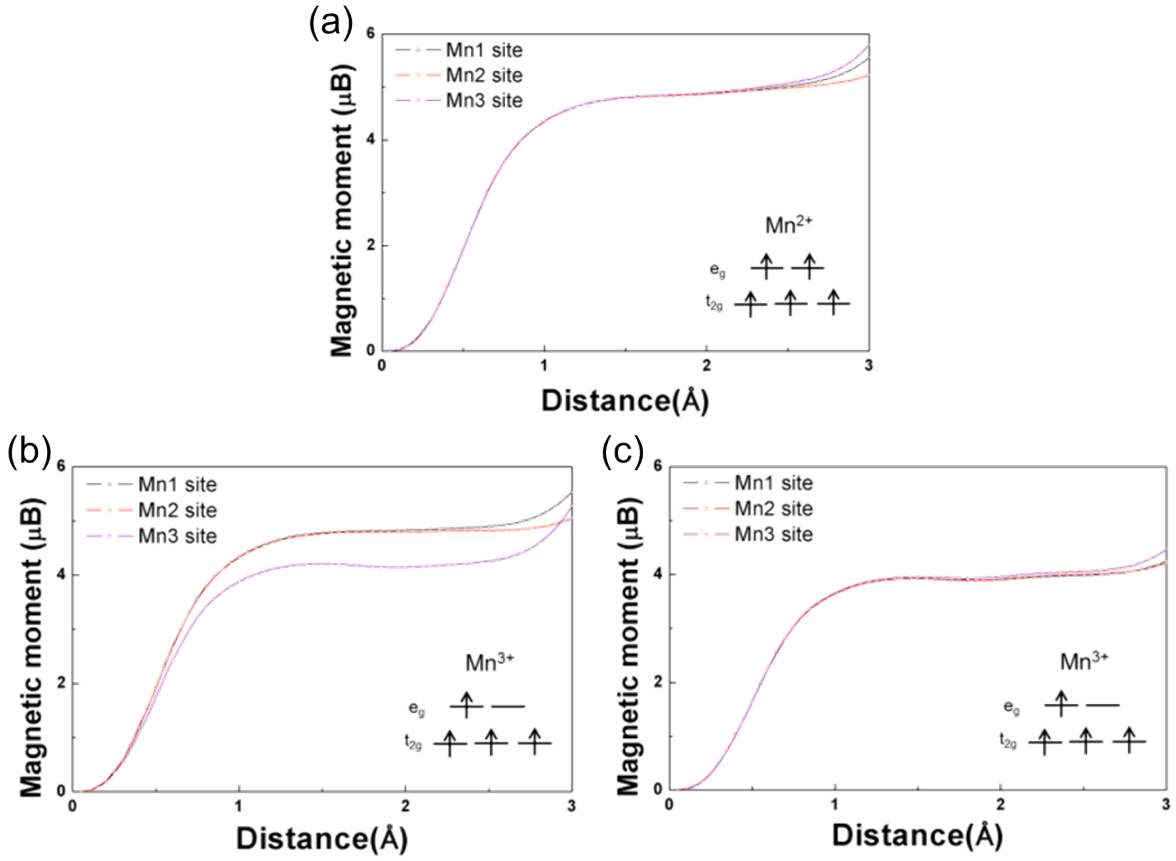

Figure S6. Spin integration of Mn ions in (a) $Na_4Mn_3(PO_4)_2(P_2O_7)$, (b) $Na_3Mn_3(PO_4)_2(P_2O_7)$ and (c) $NaMn_3(PO_4)_2(P_2O_7)$.

Table S2. Bader charge analysis on $Na_4Mn_3(PO_4)_2(P_2O_7)$ upon desodiation.

Sites	Bader charge		
	Mn1	**Mn2**	**Mn3**
$Na_4Mn_3(PO_4)_2(P_2O_7)$	+1.50	+1.50	+1.51
$Na_3Mn_3(PO_4)_2(P_2O_7)$	+1.52	+1.53	+1.74
$NaMn_3(PO_4)_2(P_2O_7)$	+1.75	+1.78	+1.78

Confirmation of Mn oxidation preference by partial Density of States (pDOS)

Fig. S7 shows the Mn pDOS of $Na_4Mn_3(PO_4)_2(P_2O_7)$, $Na_3Mn_3(PO_4)_2(P_2O_7)$ and $NaMn_3(PO_4)_2(P_2O_7)$. In $Na_4Mn_3(PO_4)_2(P_2O_7)$, all Mn ions have fully occupied up spin electrons and unoccupied down spin orbitals above 4 eV, which corresponds to the spin state of Mn^{2+}. As one Na is extracted from the structure, Mn3 up spin orbital arises above Fermi level, which indicates the absence of an up spin electron at e_g orbital. In addition, unoccupied down spin orbital of Mn3 shifts toward lower energy level, which results from the splitting of e_g level due to the Jahn-Teller distortion. Therefore, it is concluded that Mn3 in $Na_3Mn_3(PO_4)_2(P_2O_7)$ is in a 3+ charged state, as determined by spin integration and Bader charge analysis as well. In $NaMn_3(PO_4)_2(P_2O_7)$, all Mn ions are in a 3+ charged state, as they all have unoccupied up spin orbitals.

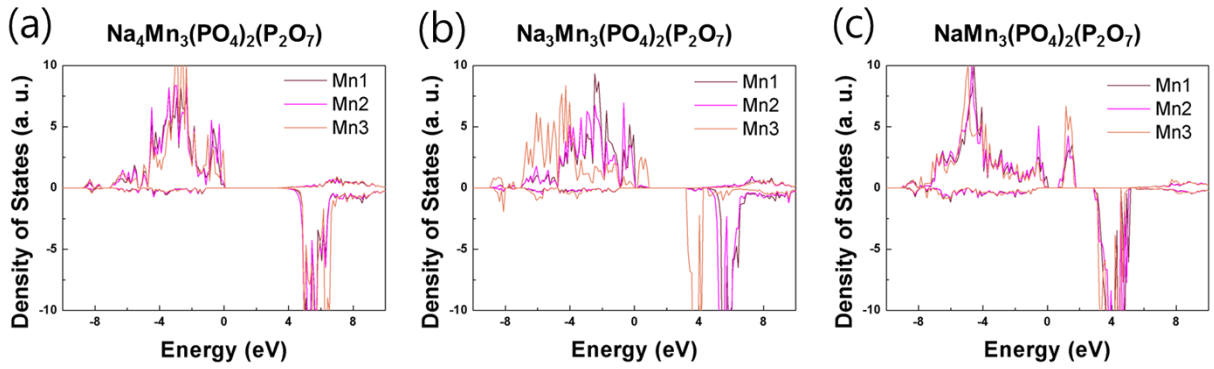

Figure S7. Partial Density of States (pDOS) of (a) $Na_4Mn_3(PO_4)_2(P_2O_7)$, (b) $Na_3Mn_3(PO_4)_2(P_2O_7)$ and (c) $NaMn_3(PO_4)_2(P_2O_7)$.

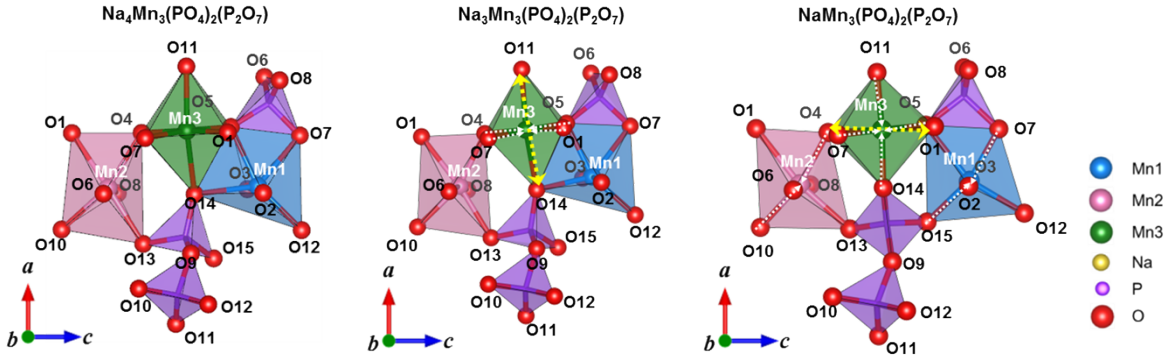

	x = 4	*x* = 3	*x* = 1		*x* = 4	*x* = 3	*x* = 1		*x* = 4	*x* = 3	*x* = 1
Mn1-O12	2.19359	2.14609	2.12345	**Mn2-O1**	2.30757	2.32009	2.34324	**Mn3-O11**	2.26099	2.26949	1.90277
Mn1-O5	2.27667	2.20061	2.34099	**Mn2-O13**	2.335	2.25696	2.22463	**Mn3-O14**	2.44977	2.41048	1.91366
Mn1-O7	2.34478	2.3876	1.96494	**Mn2-O6**	2.13627	2.1887	1.95271	**Mn3-O1**	2.14498	1.99636	2.37308
Mn1-O15	2.29278	2.21251	1.98209	**Mn2-O8**	2.1425	2.13742	1.99626	**Mn3-O4**	2.13777	1.99852	2.31788
Mn1-O3	2.15481	2.13651	1.98471	**Mn2-O10**	2.20473	2.18322	1.96033	**Mn3-O5**	2.15207	2.03149	1.96856
Mn1-O2	2.1573	2.21453	1.94916	**Mn2-O4**	2.25386	2.18287	1.96624	**Mn3-O7**	2.16584	2.00348	1.99423

Figure S8. The magnified local structure of $Na_{4-x}Mn_3(PO_4)_2(P_2O_7)$ (x = 0, 1, 3). The bond lengths between Mn and O ions are listed in the table below.

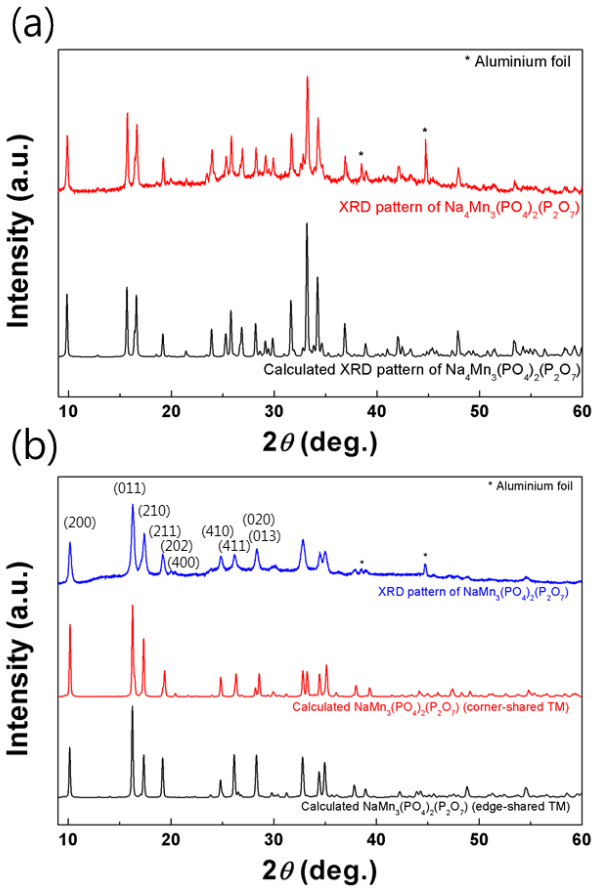

Figure S9. The XRD patterns of $Na_{4-x}Mn_3(PO_4)_2(P_2O_7)$ ((a) x = 0, (b) x = 3) from experiments and DFT calculations. The lattice parameters of simulated XRD peaks are adjusted to experimental value to address errors originated from an overestimation from first principles calculations. The simulated XRD patterns of $Na_{4-x}Mn_3(PO_4)_2(P_2O_7)$ ((a) x = 0, (b) x = 3) are well matched with that from the experiment. In the case of $NaMn_3(PO_4)_2(P_2O_7)$, two different structural models with the edge- and corner-sharing geometry of Mn1-O_6 and Mn3-O_6 polyhedra in the structure are compared, and the latter is well matched with an experimental result. Most of the peaks below 30º including (200), (011), (211), (202), (400), (410), (411) (020) and (013) show better correspondence to the experimental XRD pattern with a similar relative intensities than the former case. Also, the peaks at higher angles with low intensity also matched reasonably well with experiments.

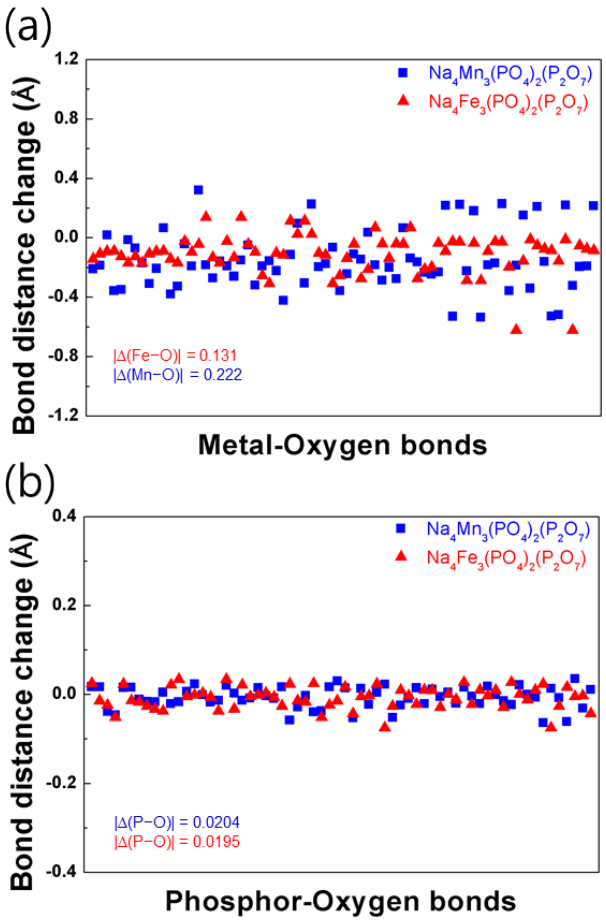

Figure S10. Bond distance change of (a) Δ(Me−O) and (b) Δ(P−O) in $Na_4Me_3(PO_4)_2(P_2O_7)$ (Me=Mn, Fe) after full charge. Average values of |Δ(Me−O)| and |Δ(P−O)| for Fe- and Mn-based electrode are presented the inset. The bond distance of Mn−O shows significant changes after full charge compared to that from Fe−O caused from Jahn-Teller distortion, while P−O bonds show small differences in both phases.

Table S3. The calculated activation barriers for Na diffusion in $Na_{4-x}Fe_3(PO_4)_2(P_2O_7)$. ($x$ = 0, 3)

From (Na site)	**To** (Na site)	$E_{a,}$ **(meV)** $Na_4Fe_3(PO_4)_2(P_2O_7)$	$E_{a,}$ **(meV)** $NaFe_3(PO_4)_2(P_2O_7)$
1	1	256	349
1	4	599	922
2	4	481	853
3	1	540	269
3	2	344	558
3	4	685	630
4	4	544	325

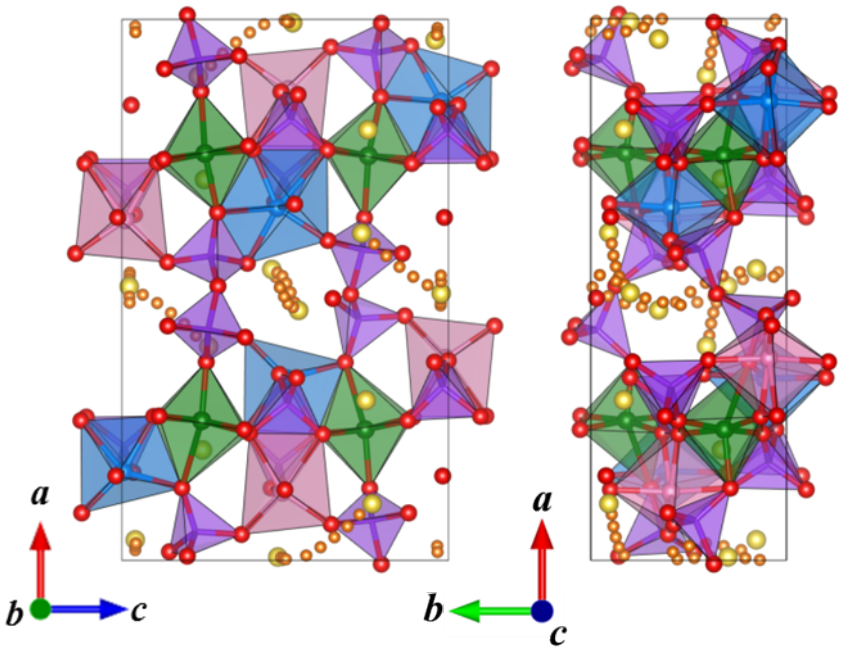

Figure S11. Na diffusion pathways in $NaFe_3(PO_4)_2(P_2O_7)$ with an activation energy below 500 meV.

Table S4. Distance from diffusing Na ions in the intermediate state to adjacent Mn ions and O ions. Details of the local structure are shown in Figure 6.

Distance from migrating Na	$Na_4Mn_3(PO_4)_2(P_2O_7)$	$NaMn_3(PO_4)_2(P_2O_7)$
Mn1	4.31(2+)	4.24(3+)
Mn2	3.62(2+)	3.81(3+)
O8	2.52	3.19
O9	2.51	2.84
O10	2.51	2.62
O12	2.83	2.38
O13	2.69	2.17
O15	2.56	2.58

Distance from migrating Na	$Na_4Fe_3(PO_4)_2(P_2O_7)$	$NaFe_3(PO_4)_2(P_2O_7)$
Fe1	4.36(2+)	4.40(3+)
Fe2	3.85(2+)	4.08(3+)
O8	2.60	-
O9	2.49	-
O10	2.38	2.93
O12	2.92	1.99
O13	2.83	2.26
O15	2.35	2.41
O6	-	2.90
O10	-	2.93

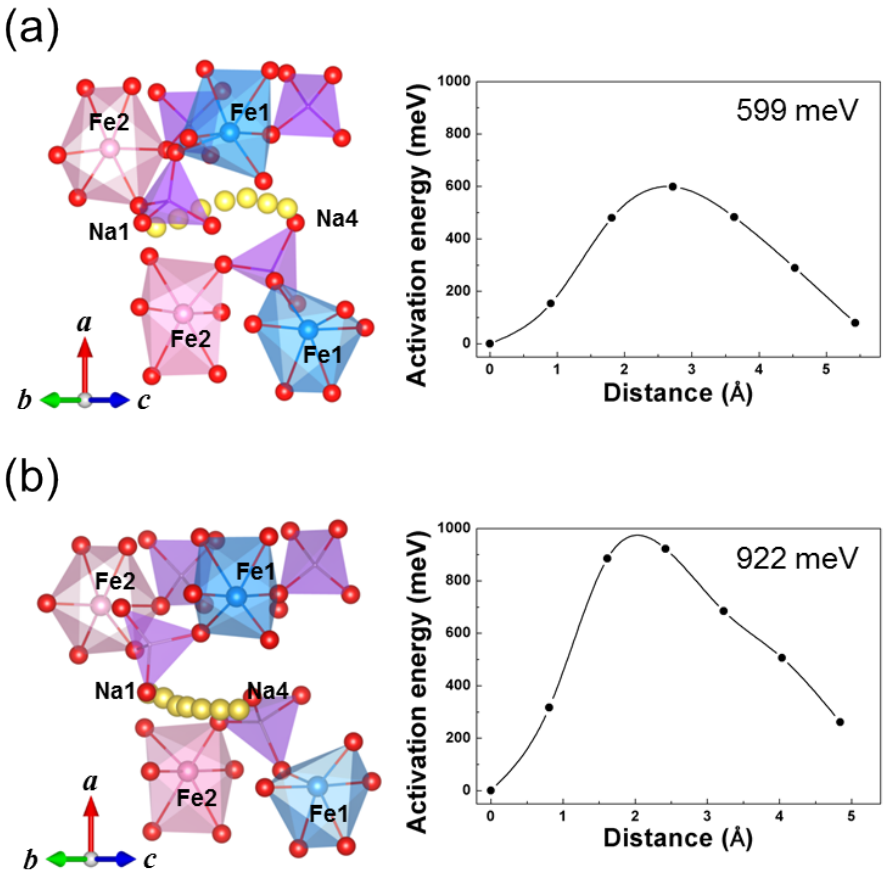

Figure S12. Magnified diffusion pathways of Na ions from Na1 to Na4 site in (a) $Na_4Fe_3(PO_4)_2(P_2O_7)$ and (b) $NaFe_3(PO_4)_2(P_2O_7)$.

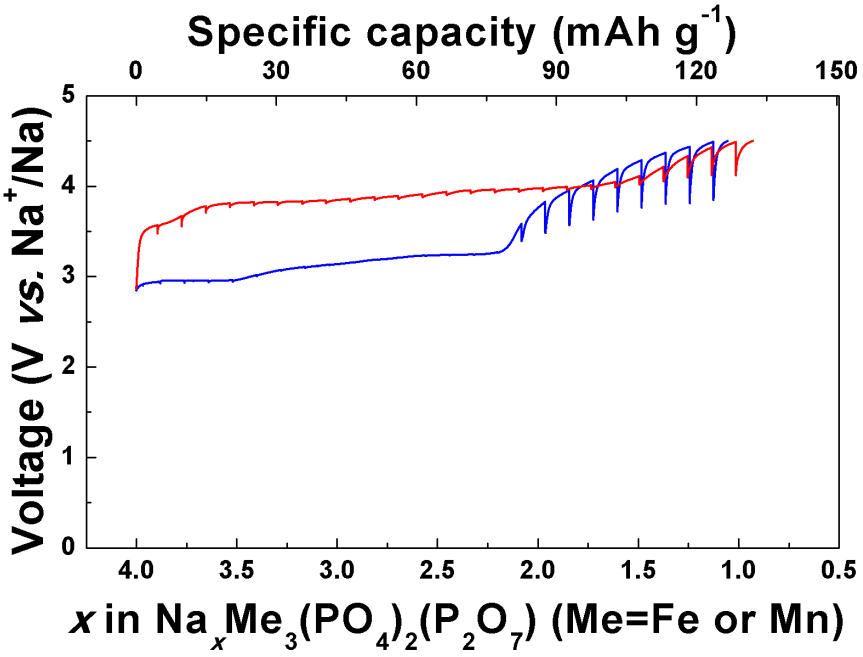

Figure S13. Galvanostatic intermittent titration technique (GITT) profiles of $NaMn_3(PO_4)_2(P_2O_7)$ and $Na_4Fe_3(PO_4)_2(P_2O_7)$ in Na-ion cells.